Chapter 24
Structural, Magnetic and Optical Study of Transition Element Doped Bismuth Ferrite

Arti, Anahat, Sumit Kumar, P. Kumar, and Vivek Verma

Abstract Enhanced structural and optical properties of pure and manganese (Mn) doped bismuth ferrite has been studied using sol–gel method as preparation technique. The scanning electron microscope analysis showed that Mn doping decreases grain size. M-H loops shows modified magnetic properties with Mn doping. The values of dielectric constants $\varepsilon' = 63.68$ and $\varepsilon'' = 12.47$ of BFO are seen to be enhanced with increase in manganese content and is maximum for $BiFe_{0.8}Mn_{0.2}O_3$ sample. The observed behaviour of ferroelectric P-E loops shows modification with increase in manganese content in BFO samples. The modified ferroelectric behaviour may results in better response of I-V characteristics i.e. dark current which leads good response in photocurrent values. Mn doping leads to the narrowing of the band gap of $BiFe_xMn_{1-x}O_3$ as evaluated from U-V visible response. Pure and Mn doped bismuth ferrite exhibited modification in leakage current from I-V characteristics, which may results in better photovoltaic response. Mn doping in BFO shows modified behavior in various properties, which makes BFO a better material for various applications.

24.1 Introduction

In recent years, due to lacking of energy resources and increasing demands of this era, natural resources of energy is the great way of harvesting energy. Solar energy is one of the most demanding natural resource of energy. From solar energy, light energy can be harvested through various techniques. One of the technique we are studying is the Photovoltaic effect. Due to unique features of $BiFeO_3$ (BFO) i.e. appropriate band gap value (~2.73 eV) and self induced polarization, it plays very crucial role in the research areas of photovoltaic, photocatalytic and in optoelectronic devices. Multiferroic is class of materials which exhibit both ferroic properties simultaneously. BFO is a multiferroic material with its unique properties, which has applications in memory

Arti (✉) · Anahat · S. Kumar · P. Kumar · V. Verma
Department of Physics, Hindu College, University of Delhi, Delhi, India

Arti · S. Kumar · P. Kumar
Department of Physics and Astrophysics, University of Delhi, Delhi, India

V. Singh et al. (eds.), *Proceedings of the International Conference on Atomic, Molecular, Optical & Nano Physics with Applications*, Springer Proceedings in Physics 271,
https://doi.org/10.1007/978-981-16-7691-8_24

devices for storing data, sensors, photovoltaics and spintronics [1]. BFO has attracted attention not only because of its magneto electric coupling but also due to its good optical properties. The materials have good ferroelectric behaviour and low value of band gap are known and being used nowadays for good photovoltaic response, because the spontaneous polarization separates the photo generated electron–hole pairs produces internal electric field and thus, enhanced the photovoltaic properties. In ferroelectric materials polarization leads self-induced polarization. It is the advantage of this self-induced polarization that PV effect in ferroelectric materials requires no p–n junction. The silicon based photovoltaic cells, have limitation of diffusion in junction based solar cell and due to their high cost. Further improvement in efficiency of solar cells is very limited. Photovoltaic effect in $BiFeO_3$ perovskite solar cell and modification in efficiency can be optimized by doping with suitable elements in bismuth ferrites and their composites with suitable magnetic and ferroelectric materials [2]. In this work Bismuth ferrite (BFO) and manganese doped Bismuth ferrite samples are prepared using sol–gel method. Increasing doping of Mn content enhanced the following properties i.e. ferroelectric, magnetic and optical properties, and also the increased content of manganese shows effect on crystal structure and decreased impurities [3].

24.2 Experimental Method

Low temperature synthesis of Pure and manganese doped BFO samples has been done by sol–gel method. In this method Bismuth nitrate [$Bi(NO_3)_3{\cdot}5H_2O$], iron nitrate [$Fe(NO_3)_3{\cdot}9H_2O$], and manganese acetate [$Mn(CH_3COO)_2{\cdot}4H_2O$], were added for making gel according to stoichiometry amount [4]. All the nitrates were allowed for stirring maintaining the magnetic stirring, to make a homogeneous solution. Oxalic acid is then added as complexing agent in the precursor solution. Then obtained solution was allowed to heat for obtaining gel. During heating the amount of gases released and the gel coverts to powder. Powder was then grinded well and sintered at 500 °C for 4 h for phase formation. Further pellets were made for making measurements of different powder samples.

24.3 Results and Discussion

24.3.1 Structural Properties

Figure 24.1 shows XRD spectra of pure and Mn doped BFO samples. From Fig. 24.1 it can be observed that all pure and doped BFO samples exhibits polycrystalline behaviour.

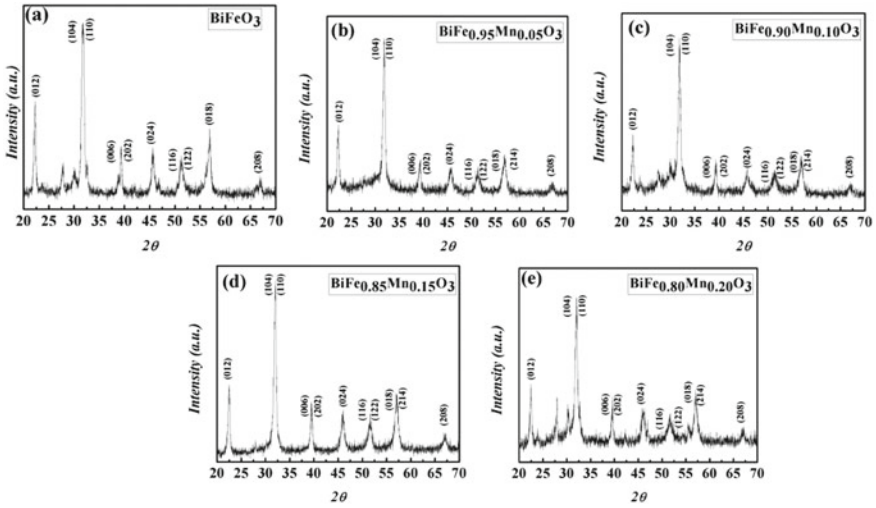

Fig. 24.1 XRD spectra of pure and doped samples of BFO

Apart from the main $BiFeO_3$peaks few minor peaks belonging to $Bi_{25}FeO_{29}/Bi_2O_3$are visible in the 2θ range between 25 and 30. The plane (1 0 4), (1 1 0) and (0 0 6), (2 0 2) shown in the Figure are showing the peaks of all the samples which are merging from doublet peak to singlet peak with increase in Mn content may cause change in the structure. This structural transition in the ceramics may be due to substitution of Fe^{3+}cations with Mn^{2+}cations. The variation in structural parameter for R3c space group is observed with Mn substitution. It can depict from Table 24.1 that higher the Mn content for $x = 0.05$ to 0.20 induce larger unit cell volume. Thus the shifting of peaks (104) and (110) towards lower angles (Fig. 24.1), may be due to structural transition to orthorhombic from rhombhohedral structure. Due to lager radii of Mn and its substitution at B-site Fe cation which has smaller radii, the cationic radius of B-site increases. The value of tolerance factor 't' gives the reason for change in cationic radius. With doping content of Mn the value of tolerance factor is increasing as shown in Table 24.1. Tolerance factor for $BiFe_{1-x}Mn_xO_3$ is given by, $t = R_A + R_O/1.44(R_B + R_O)$, where R_A is the effective ionic radii of Bi^{3+}, R_B is the effective radii of Fe^{3+}, and R_O is the effective radii of O^{2-}ions. If 't < 1', the

Table 24.1 Tolerance factor, crystallite size and grain size of samples

Sample name	Tolerance factor (t)	Crystallite size (d) (nm)	Grain size (SEM) (nm)
$BiFeO_3$	0.88729	12.7	81.30
$BiFe_{0.95}Mn_{0.05}O_3$	0.89337	17.9	59.45
$BiFe_{0.90}Mn_{0.10}O_3$	0.89958	18.8	54.73
$BiFe_{0.85}Mn_{0.15}O_3$	0.90584	16.2	50.60
$BiFe_{0.80}Mn0._{20}O_3$	0.93023	21.6	48.63

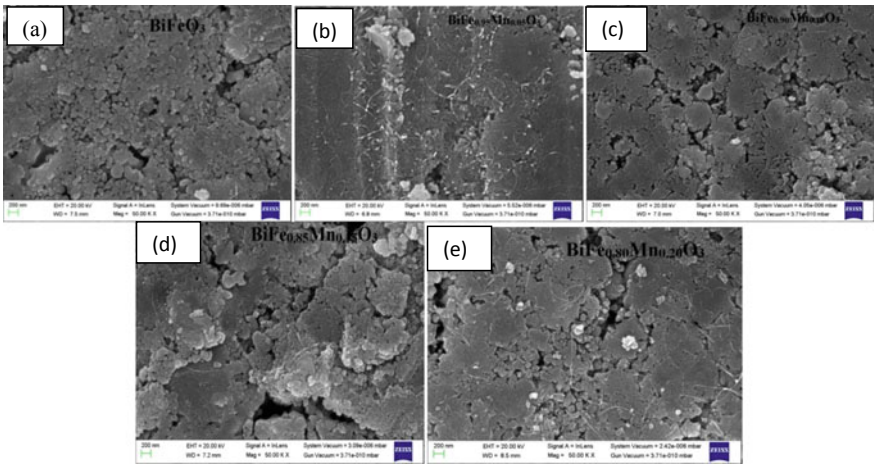

Fig. 24.2 SEM micrographs of pure and doped BFO samples

strain induces lattice distortion because the strain acts on the bond of BFO i.e. Fe–O and Bi-O bonds which leads phase change such as orthorhombic or tetragonal. This corresponds the phase transition from rhombohedral to orthorhombic with increase in manganese content in bismuth ferrite. This leads to suppression of rhombohedral phase and may results new crystallographic phases [5]. This change in crystal structure of $BiFe_{1-x}Mn_xO_3$ ceramics may affect its various properties, which will be useful for various applications. SEM micrographs of pure and doped BFO samples has been shown in Fig. 24.2. Distribution and average size of grain for all the samples has been calculated using Image j software. Grain size decreases with increase in doping content of Mn in BFO (~81.30 nm to 48.63 nm). The decrease in grain size is may be due to different ionic radii of Mn^{2+} and Fe^{3+}. Another reason for grain size decrement is may be because of Kirkendal effect [6].

24.3.2 Ferroelectric Studies

P-E loops for pure and doped BFO ceramics has been shown in Fig. 24.3. It is observed that the polarization (P) and coercivity (E_c) enhanced with doping content of Mn in BFO. This modification in the ferroelectric properties is may be due to decrease in grain size and phase transformation. Pure BFO sample shows lossy nature with small value of polarization (0.3804 $\mu C/cm^2$) which leads to large leakage current. With increase of Mn content in BFO, the value of polarization increases up to the value of $Ps = 5.95\ \mu C/cm^2$, for $Mn = 0.15$. It could not be measured the P-E loop hysteresis behavior for the sample $Mn = 0.20$ due to its high leakage behavior. This change in polarization value with doping content of Mn is may be due to lattice distortion of BFO samples [7, 8].

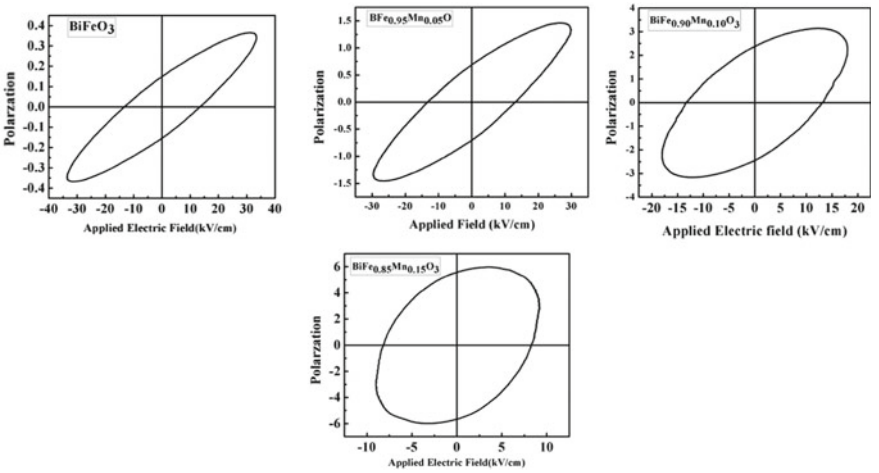

Fig. 24.3 Room temperature P-E loops for pure and doped BFO samples

24.3.3 Dielectric Properties

Dielectric properties of prepared samples of pure and Mn doped BFO has been studied. The value of dielectric constants both real and imaginary parts increases with Mn content in BFO as shown in the Table 24.2. With increasing value of frequency the dielectric constant, both parts of permittivity (real and imaginary) of pure and doped BFO ceramics decreases and at higher frequencies permittivity becomes independent. Thus, low frequency dispersion seen in the results may be due to Maxwell–Wagner effect or interfacial polarization which satisfies Koop's theory. Secondly, at low frequency, hopping of electron is not possible due of lack of energy, so to give sufficient energy the frequency of electric field has been increased and then at some point electrons get sufficient energy for hopping from Fe^{+2} to Fe^{+3} ions. Due to hopping of ions the conductivity of dielectrics increases with frequency, and hence

Table 24.2 Magnetic, dielectric, ferroelectric properties for pure and doped BFO samples

Sample name	Magnetization (M_s)	Dielctric constant				Ferroelectric properties	
		1000 Hz		10^5 Hz			
		ε'	ε''	ε'	ε''	Polarization P_s ($\mu C/cm^2$)	Coercivity E_c (kV/cm)
$BiFeO_3$	0.1581	63.28	5.21	51.30	2.64	0.357	13.001
$BiFe_{0.95}Mn_{0.05}O_3$	0.1746	81.66	26.52	62.48	3.74	1.363	13.258
$BiFe_{0.90}Mn_{0.10}O_3$	0.1614	116.81	152.22	60.89	10.13	2.682	13.222
$BiFe_{0.85}Mn_{0.15}O_3$	0.1647	122.41	169.27	44.11	10.13	3.749	8.317
$BiFe_{0.80}Mn_{0.20}O_3$	0.1676	159.16	497.37	57.69	27.17	–	–

decrements occur in dielectric constant. The dielectric constant and loss tangent of BFMnO is larger at low frequencies. This can be ascribed to Oxygen vacancies created by the substitution of Mn for Fe ions. Since Mn can be stable in two ionic state (Mn^{2+} and Mn^{3+}) which can create oxygen vacancies in the compound. Dielectric losses decrease with increase in frequency and similar is the case with loss tangent [9, 10].

24.3.4 Magnetic Properties

Table 24.2 diminutive enhancement in magnetization for pure and doped BFO ceramics. Weak ferromagnetic behaviour has been exhibited by the prepared ceramics of pure and doped BFO. Pure BFO exhibits G-type antiferromagnetic behaviour. Enhanced magnetic properties of all the BFO samples may be due to Mn doping and decrease in average particle size. Tilt in octahedral and formation of canted structure may be due to lager ionic size of manganese than iron. So Fe–O-Fe bond angle and Fe–O length has been affected due to the presence of manganese ions in BFO. Thus enhanced magnetization results following this phenomenon explained above [11, 12].

24.3.5 FTIR

FTIR spectra of Pure and doped BFO has been shown in the Fig. 24.4. The changes (molecular and chemical) in BFO structure as reported above due to changes in Fe–O due to doping of any other element are shown by FTIR spectra. The broad absorption peaks below 1000 cm^{-1} shows the vibrations of bonds Bi–O or Fe–O. In this work we observed peak near 565.33 due to the vibrations of Fe–O and Bi–O groups. The broad peak near 560 $cm^{-1}$is at may be due to Fe–O and Bi-O stretching of FeO_6 and BiO_6 octahedral [22]. The low intensity peak near 2929.43 cm^{-1} in the samples may also be due to the vibrations (-OH) groups. Another broad weak absorption peaks near 111.85 and 1672 cm^{-1} may be due to the groups of citric, tartric and oxalic acid. The observed IR peaks at 1370 cm^{-1} may shows the bending vibration of C–H. Mn concentration increases small amount of splitting in some of the peaks near 565.23 and 111.85 cm^{-1} and 1370.11 cm^{-1}. The splitting of absorption peaks for some of the samples may be due to the distortion in BFO caused by structural transition produced by Mn substitution, can also be verified by XRD spectra [13–15].

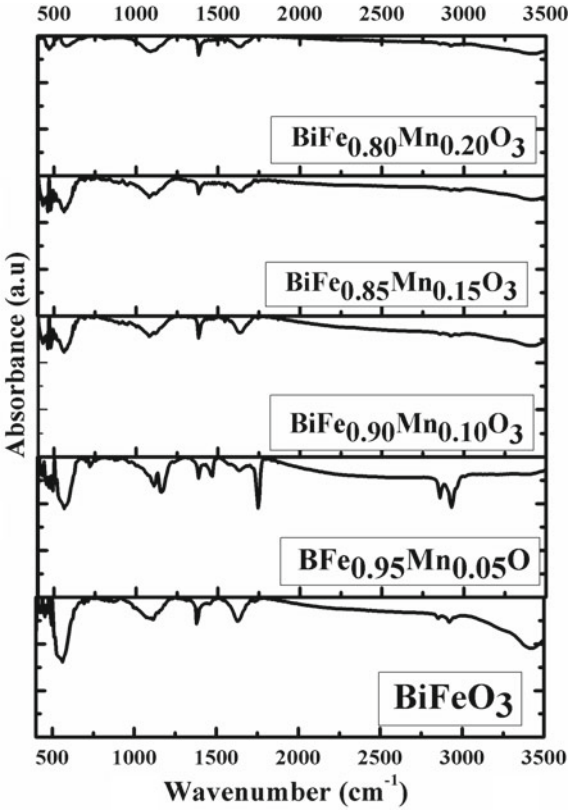

Fig. 24.4 FTIR spectra of pure and doped BFO samples

24.3.6 Photovoltaic Properties

24.3.6.1 Band-Gap

The band-gap of pure and magnese doped samples of BFO were studied in the UV–vis wavelength range of 400–600 nm. The corresponding energy band gap of pure and doped samples has been calculated from Tauc's relation for direct band gap. The estimated bandgap values were estimate ~2.37–2.00 eV for $BiFe_{1-x}Mn_xO_3$ samples. Decrement in energy band gap values has been observed increase in manganese content in BFO. This narrowing of band gap is may be due to modification n the value of lattice constants and particle size which leads alteration of the band structure of BFO [16–18].

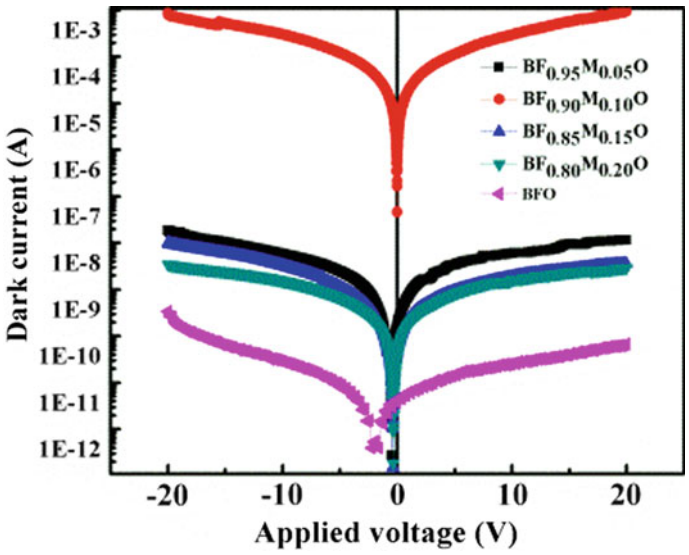

Fig. 24.5 I-V characteristics of Pure and doped BFO samples

24.3.6.2 I-V Characteristics

Figure 24.5 shows the studies of I-V characteristics of bismuth ferrite (BFO) and manganese doped bismuth ferrite samples. Room temperature measurements of dark current has been done for pure and doped BFO samples at room temperature. Leakage current for pure BFO is $I_{dark} = 2.12 \times 10^{-8}$A, and leakage current increases with increase in Mn content in BFO. It can be verified by P-E loops or ferroelectric data which shows lossy behavior. The observed P-E loops shows the consistency with the leakage current behaviour of samples. This leakage current phenomenon can be understood on the basis of some phenomenon such as bulk limited Poole–Frenkel emission (PF) mechanism, or interface-limited Schottky emission, the bulk-limited space-charge-limited conduction (SCLC) mechanism,. This lowering of leakage current values implies good ferroelectric response, and more inherent polarization in the sample which is beneficial for good photovoltaic properties [19–22].

24.4 Conclusion

Low temperature pure and Manganese doped BFO powders has been synthesized by sol–gel method. In this work the structural, electric, magnetic and optical are studied. The phase transition and structural deformation from pervoskite rhombohedral to orthorhombic phase was shown by XRD pattern and other parameters calculated from XRD. Modification in ferroelectric and magnetic properties has been observed

which were in agreement with XRD and SEM data. The modified electrical properties results in lowering of band gap and leakage current as compared to pure BFO with increase in Mn content. Enhanced optical response of BFO with Mn doping can be beneficial for photovoltaic applications in ferroelectric materials.

References

1. A. Manzoor, A.M. Afzal, N. Amin, M.I. Arshad, M. Usman, M. N. Rasool, M. F. Khan, Article in Ceramics International (2016). https://doi.org/10.1016/j.ceramint.2016.04.083
2. M. Alexe, D. Hesse (2011). https://doi.org/10.1038/ncomms1261
3. H.M. Xu, H. Wang, J. Shi, Y. Lin, Photoelectrochemical performance observed in Mn-doped $BiFeO_3$ hetero structured thin films. Cewen Nan Nanomaterials **6**, 215 (2016)
4. *Preparation and Characterization of Bismuth Ferrite Nanoparticle Using Sol–Gel Method*. https://www.researchgate.net/publication/325012631. https://doi.org/10.22214/ijraset.2018.4299
5. V. Srinivas, A.T. Raghavender, K. Vijaya Kumar Volume (2016), Article ID 4835328, 5 pages https://doi.org/10.1155/2016/4835328
6. B. Dhanalakshmi, K. Pratap, B. Parvatheeswar Rao, P.S.V. Subb Rao. 193–201, 676 (2016). https://doi.org/10.1016/j.jallcom.2016.03.208
7. Nisha, D.K. Shukla, S. Kumar, Ferroelectric and dielectric properties of Mn doped BiFeO3 bulk ceramics. AIP Conf. Proc. **2006**, 030037 (2018)
8. J.Z. Huang, Y. Shen, M. Li, C.W. Nan, J. Appl. Phys. **110**, 094106 (2011)
9. C. Elissalde, J. Ravej, Mater. Ceram. Int. **39**, 8527 (2013)
10. S. Godara, B. Kumar, Ceramic Intern. **41**, 6912 (2015)
11. C.T. Munos, J.P. Rivera, H. Schmid, Ferroelectrics **55**, 235 (1984)
12. J.P. Tae, C. Georgia, J.V. Arthur, M.R. Arnold, S.W. Stanislaus, Nano. Lett. **7**, 766 (2007)
13. M.M. Kumar, A. Srinivas, S.V. Suryanarayana, J. Magn. Magn. Mater. **188**, 203 (1998)
14. R. Mazumder, P.S. Devi, D. Bhattacharya, P. Choudhury, A. Sen, M. Raja, Appl. Phys. Lett. **91**, 3 (2007)
15. Y. Hu, L. Fei, Y. Zhang, J. Yuan, Y. Wang, H. Gu, J. Nanomater. **2011**, 6
16. D. Suastiyanti, Ismojo, Int. J. Eng. Sci. (IJES) **5**, 114–117 (2016)
17. H.M. Xu, H. Wang, J. Shi, Y. Lin, Cewen Nan Nanomaterials **6**, 215 (2016)
18. R.Q. Guo, L. Fang, W. Dong, F.G. Zheng, M.G. Shen, J. Phys. Chem. C, **114**, 21390 (2010)
19. F. Gao, X.Y. Chen, K.B. Yin, S. Dong, Z.F. Ren, F. Yuan, T. Yu, Z.G. Zou, J.M. Liu, Adv. Mater. **19**, 2889 (2007)
20. Y.L. Pei, C. Zhang, J. Alloy. Compd. **570**, 57 (2013)
21. H. Yang, M. Jain, N.A. Suvorova, H. Zhou, H.M. Luo, D.M. Feldmann, Q.X. Jia, Appl. Phys. Lett. **91**, 072911 (2007)
22. G.W. Pabst, L.W. Martin, Y.H. Chu, R. Ramesh, Appl. Phys. Lett. **90**, 072902 (2007)